

Chemical Shift: The Artifact and Clinical Tool Revisited¹

Maureen N. Hood, BS

Vincent B. Ho, MD

James G. Smirniotopoulos, MD

Jerzy Szumowski, PhD

LEARNING OBJECTIVES

After reading this article and taking the test, the reader will be able to:

- Describe the chemical shift artifact and where it is typically seen on MR images.
- Identify ways to minimize or exaggerate the chemical shift artifact.
- Give examples of common body and neurologic pathologic conditions for which the use of chemical shift imaging can be advantageous.

The chemical shift phenomenon refers to the signal intensity alterations seen in magnetic resonance (MR) imaging that result from the inherent differences in the resonant frequencies of precessing protons. Chemical shift was first recognized as a misregistration artifact of image data. More recently, however, chemical shift has been recognized as a useful diagnostic tool. By exploiting inherent differences in resonant frequencies of lipid and water, fatty elements within tissue can be confirmed with dedicated chemical shift MR pulse sequences. Alternatively, the recognition of chemical shift on images obtained with standard MR pulse sequences may corroborate the diagnosis of lesions with substantial fatty elements. Chemical shift can aid in the diagnosis of lipid-containing lesions of the brain (lipoma, dermoid, and teratoma) or the body (adrenal adenoma, focal fat within the liver, and angiomyolipoma). In addition, chemical shift can be implemented to accentuate visceral margins (eg, kidney and liver).

Abbreviations: FMPSGR = fast multiplanar spoiled gradient echo, TE = echo time

Index terms: Magnetic resonance (MR), artifacts • Magnetic resonance (MR), chemical shift • Magnetic resonance (MR), tissue characterization

RadioGraphics 1999; 19:357-371

¹From the Department of Radiology and Nuclear Medicine, Uniformed Services University of the Health Sciences, 4301 Jones Bridge Rd, Bethesda, MD 20814-4799 (M.N.H., V.B.H., J.G.S.) and the Department of Radiology, Oregon Health Sciences University, Portland (J.S.) Recipient of a Certificate of Merit award for a scientific exhibit at the 1997 RSNA scientific assembly. Received March 10, 1998; revision requested May 5 and received July 16; accepted July 16. **Address reprint requests to M.N.H.**

The opinions or assertions contained herein are the private views of the authors and are not to be construed as official nor as reflecting the views of the Uniformed Services University of the Health Sciences or the Department of Defense.

©RSNA, 1999

Figure 1. Equation illustrates the relationship between chemical shift and field strength, where Δf_{cs} = resonant frequency shift in parts per million (ppm), δ = relative chemical shift frequency difference, and ω_0 = main magnetic field resonant frequency. Given that human lipid and water have a resonant frequency difference of 3.5 ppm (ie, $\Delta f_{cs} = 3.5$ ppm), the chemical shift frequency change (δ) will be approximately 224 Hz at a field strength of 1.5 T (ie, $\omega_0 = 64$ MHz).

$$\Delta f_{cs} = \delta \cdot \omega_0$$

$$\delta = \Delta f_{cs} / \omega_0$$

$$\begin{aligned} \delta &= 3.5 \text{ ppm} / 64 \text{ MHz} \\ &= 224 \text{ Hz} \end{aligned}$$

■ INTRODUCTION

Phenomena that may result in image artifacts can sometimes be used to assist in radiologic diagnosis. Chemical shift is an example of such a phenomenon in magnetic resonance (MR) imaging. Chemical shift refers to the signal alterations that result from the inherent differences in the resonant frequencies of precessing protons. Clinically, the chemical shift phenomenon is most evident between the signals of water and lipid. Chemical shift is a complicated phenomenon and is probably best known, or more precisely, notorious for its ability to cause misregistration of MR image data. This effect, also referred to as chemical shift artifact, results from the mismapping of water and lipid signals and is most commonly encountered when one images fluid-filled structures such as the orbits or bladder, which are enveloped within fatty tissue (1-3).

Only recently, chemical shift has been recognized as a diagnostic aid, possibly as a result of the growing experience with faster gradient-echo pulse sequences or of the increased clinical use of MR imaging (4). When pulse sequences are modified to be sensitive to chemical shift effects, MR imaging can be used to confirm the presence of fat within lesions, a finding that can result in a definitive diagnosis. In addition, chemical shift can be used to accentuate the fat-water interfaces that occur at many visceral margins. This technique can improve the evaluation of peripheral tumors for possible extravisceral extension or the visualization of visceral contours.

In this article, the basic principles of chemical shift and their implications for clinical imaging are reviewed. Specific applications of chemical shift as a diagnostic tool in neurologic and body imaging are illustrated.

■ BASIC PHYSICS OF CHEMICAL SHIFT

● Physical Basis

When an external magnetic field is applied to tissue, its nuclei will resonate at a specific frequency that depends on the strength of that external magnetic field (B_0) and its local microenvironment. The effects of the external magnetic field can be determined by the Larmor equation: $\omega_0 = \gamma \cdot B_0$, where ω is the resonant or precessional frequency and γ is the gyromagnetic ratio for a specific nuclear species (5). The effects of the local environment on the individual precessional frequency of each nucleus are further influenced by the electron shell interactions of each nucleus with those of surrounding molecules. These additional electron shell interactions influence the local magnetic shielding of the protons, creating "effective" local magnetic field strengths (B_{eff}) that have the ultimate control over the "effective" precessional frequencies (ω_{eff}), as shown by the modified Larmor equation: $\omega_{eff} = \gamma \cdot B_{eff}$ (6,7).

The molecular interactions that determine B_{eff} form the basis for the chemical shift phenomenon (5). When the chemical environments of adjacent nuclei are dramatically different in their electron (ie, magnetic) shielding, a shift in the precessional frequencies of the nuclei can occur (6). If these precessional frequency shifts are large enough, a measurable

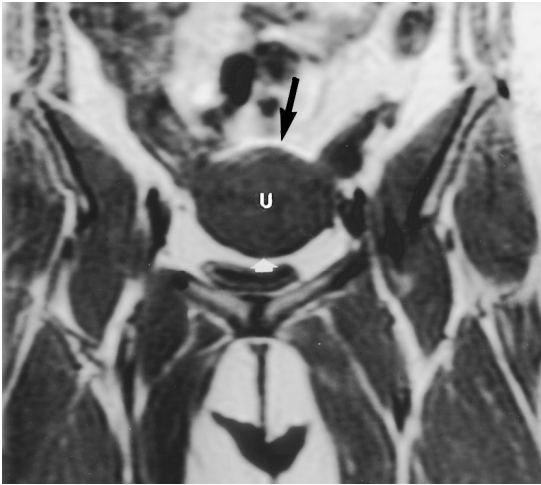


Figure 2. Coronal T1-weighted spin-echo image (repetition time msec/TE msec = 666/10) of a 52-year-old woman with an anteverted uterus demonstrates a chemical shift artifact around the uterus. The superior border of the uterus (*U*) has a bright band (black arrow), whereas the inferior border of the bladder has a dark band (white arrow). The severe lipid-water interface between the uterus and the pelvic fat produces a strong shift of the protons at the margin of the bladder.

alteration in MR signal intensity will be observed. When imaging parameters (eg, in gradient-echo sequences, the time at which the echo is sampled [ie, echo time or TE]) are manipulated, the precessional frequency shifts, or chemical shift phenomenon, can be accentuated to generate visible differences between lipid and water protons in tissue (5).

In clinical imaging, hydrogen protons form the basis for MR image signal and contrast. The chemical shift phenomenon is most noticeable between the hydrogen protons of lipid and those of water because of their large relative differences in magnetic shielding. The difference in resonant frequencies between lipid and water protons increases proportionately with the static magnetic field strength. The approximate chemical shift between human lipid (methylene $[\text{CH}_2]_n$ of fatty acids) and water is 3.5 parts per million

(5,8-11). At a field strength of 1.5 T, this shift translates to approximately a 224-Hz separation between the resonant frequencies of fat and water protons (Fig 1).

● Clinical Implications

Spatial Misregistration: The Artifact.—The inherent differences in precessional frequencies between fat and water protons have several implications in clinical imaging. The oldest and best characterized effect of chemical shift is that of spatial misregistration. Frequency and phase components of MR signal arising from a tissue are used to encode the x- and y-axis spatial coordinates of the two-dimensional section (6). Because the frequency displacement caused by chemical shift cannot be differentiated from intended spatial frequency encoding, misregistration of the resultant signal may occur along the frequency-encoding direction (also called readout axis) (6). If the MR imager is tuned or centered to the frequency of water, fat will be shifted or spatially mismatched relative to its true spatial location. This mismatching occurs throughout the image, although it is most apparent between regions that are primarily fatty and those that are composed of water or fluid (ie, at lipid-water interfaces) (5,6). When the chemical shift misregistration is greater than or equal to the size of an individual pixel, a dark or bright band of signal intensity will occur at the lipid-water interface in the frequency-encoding direction of the image (11). This pixel-by-pixel misregistration along the frequency-encoding direction visibly manifests itself as a bright or dark band running perpendicular to the frequency-encoding direction. Clinically, the chemical shift artifact is most often recognized at the margins of predominantly fluid-filled structures that are embedded in fatty regions, such as the bladder (Fig 2) and orbits (2,3,5,11). The misregistration of signal along the frequency-encoding direction

results from the erroneous mapping of the signal of the fatty elements relative to that of the fluid-filled structures. This misregistration results in the production of dark or bright bands at the lipid-water interface (Fig 3). The dark bands result from the shifting of the lipid proton signals to a lower frequency, away from the actual lipid-water interface, which causes a signal void (Fig 4) (5,6,12). The bright bands result from the overlapping of water signal with “shifted” lipid signal on the high-frequency side of the interface (Fig 4). The bright bands, although present, may be more difficult to appreciate when the object being imaged has a curved surface (6,12).

There are several ways to minimize the spatial misregistration caused by the chemical shift artifact, including choice of frequency-encoding direction, field of view, and receiver bandwidth and use of fat-suppression techniques. The size (width of dark and bright bands) and location of the chemical shift artifact are influenced by a number of factors. Most important is the selection of the frequency-encoding direction. The clinical significance of the chemical shift artifact can be reduced by choosing the frequency-encoding direction in the plane with the narrowest lipid-water interface or by selecting a direction that minimizes the chemical shift effect over the area of primary interest (Fig 5).

The imaging field of view is an operator variable that can easily be controlled and has a strong influence on the size of the chemical shift artifact seen in an image. The artifact can be minimized by decreasing the field of view (5,9).

Receiver bandwidth is another imaging parameter that may affect the amount of chemical shift artifact seen in routine MR images. The artifact is usually not readily apparent in spin-echo images unless the receiver bandwidth is



Figure 3. Coronal T1-weighted fast multiplanar spoiled gradient-echo (FMPSPGR) image (repetition time msec/TE msec, flip angle = 103/5.6, 80°) obtained with right-to-left frequency encoding of a 61-year-old man demonstrates chemical shift artifact in many of the abdominal lipid-water interfaces. Dark bands (arrowheads) are seen along the lateral right psoas muscle, lateral right renal, medial splenic, and medial left renal margins. Bright bands are visualized at the opposing lipid-water interfaces of the lateral left psoas muscle, medial right renal, lateral splenic, and lateral left renal margins.

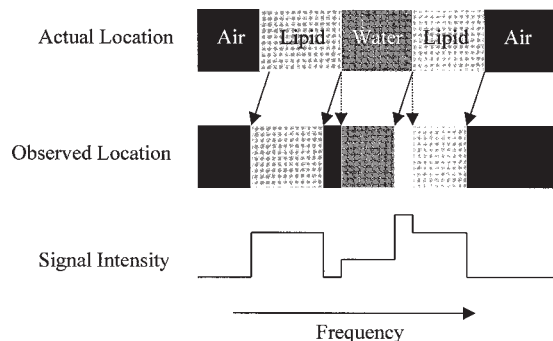


Figure 4. Schematic depicts chemical shift along the frequency-encoding direction. Lipid signal is shifted to a lower-frequency position when it is surrounded by water, which leaves a signal void (dark band) on the high-frequency side of the lipid structure and an increase in signal (bright band) on the low-frequency side.

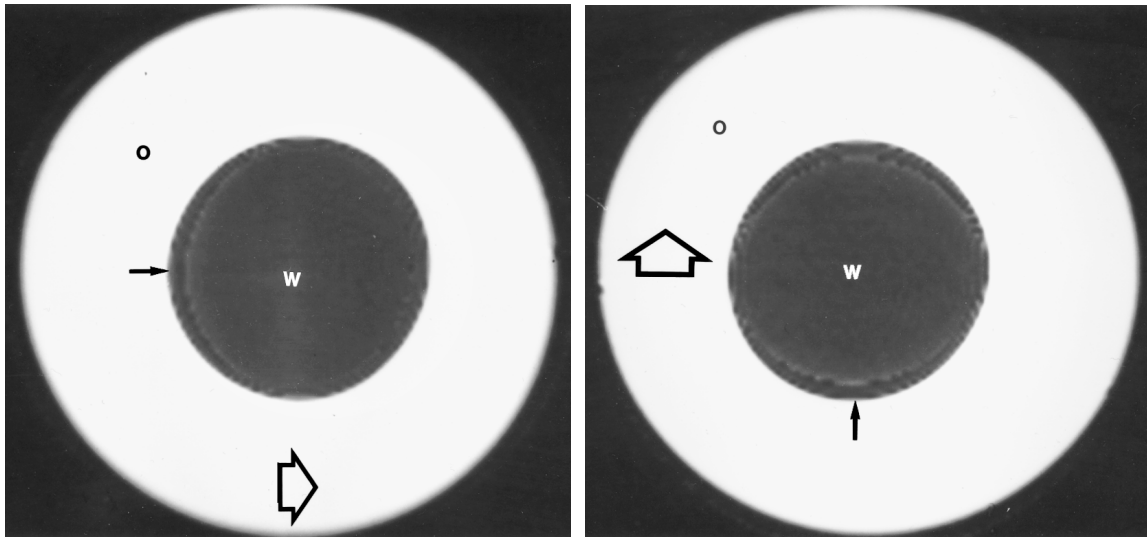


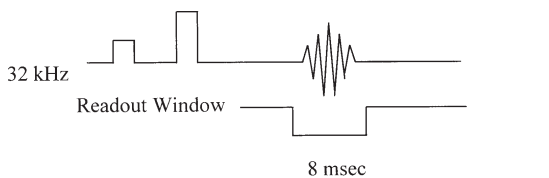
Figure 5. T1-weighted FMPSR images (51/2.1, 90°) of a phantom with inner water (*w*) and outer oil (*o*) components illustrate the chemical shift artifact, which is perpendicular to the frequency-encoding direction. **(a)** On the image obtained with left-to-right frequency encoding (open arrow), the dark band of the chemical shift artifact is noted along the superior-to-inferior water-oil interfaces (solid arrow). **(b)** On this image, the frequency encoding is switched to inferior to superior (open arrow), and the dark band of the artifact is noted along the right-left water-oil interfaces (solid arrow). The bright band is poorly visualized in both images because it is superimposed over the already bright signal of the surrounding oil.

$$\text{Chemical shift distance} = \frac{\text{Frequency shift (Hz)} \cdot \text{FOV (mm)}}{\text{Bandwidth (Hz)}}$$

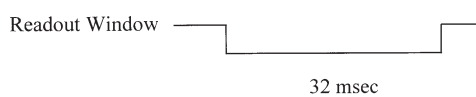
Assume: 25 cm FOV, 16 kHz BW, and a 1.5 Tesla MR scanner

$$\text{Chemical shift} = \frac{224 \text{ Hz} \cdot 250 \text{ mm}}{16,000 \text{ Hz}} = 3.5 \text{ mm}$$

6.



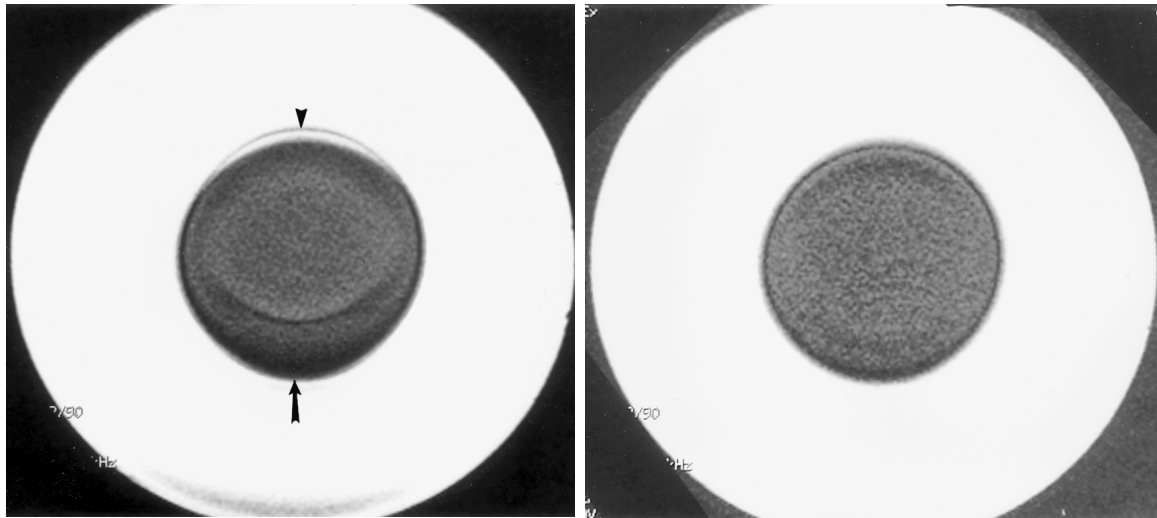
8 kHz



7.

Figures 6, 7. (6) Equation demonstrates the relationship between chemical shift, frequency shift, field of view (*FOV*), and bandwidth. (7) Pulse sequence diagram shows the differences in readout (frequency) window length with a change in the receiver bandwidth. The readout window must be open longer to preserve the field of view, which in turn, increases the chemical shift artifact.

narrowed to less than the typical ± 16 kHz. When a narrow bandwidth is used, the strength of the gradients along the frequency-encoding direction is reduced (5,9,10). The readout (frequency) window must remain open proportionally longer to preserve the field of view; thus, the apparent shift in resonant frequencies between lipid and water protons becomes more widely separated spatially (Figs 6, 7) (9,10). The effect of bandwidth on chemical shift is directly proportional to the static magnetic field strength. When using MR imaging units with 1.5 T (or greater) magnetic field strength, the operator must be very careful when narrowing the bandwidth to image anatomic areas with lipid-water interfaces because this action will increase the degree of chemical shift artifact in the resultant images (Fig 8) (2).



a.

b.

Figure 8. T1-weighted FMPSPGR images (51/2.1, 90°) of a phantom with inner water and outer oil components illustrate the effect of bandwidth on the degree of chemical shift seen in images. **(a)** This image, obtained with a bandwidth of 7.8 kHz, shows a dark band on the inferior border (arrow) and a bright band on the superior border (arrowhead) of the water portion of the phantom. **(b)** On this image, obtained with a 31.2-kHz bandwidth, the dark and bright chemical shift bands are barely noticeable.

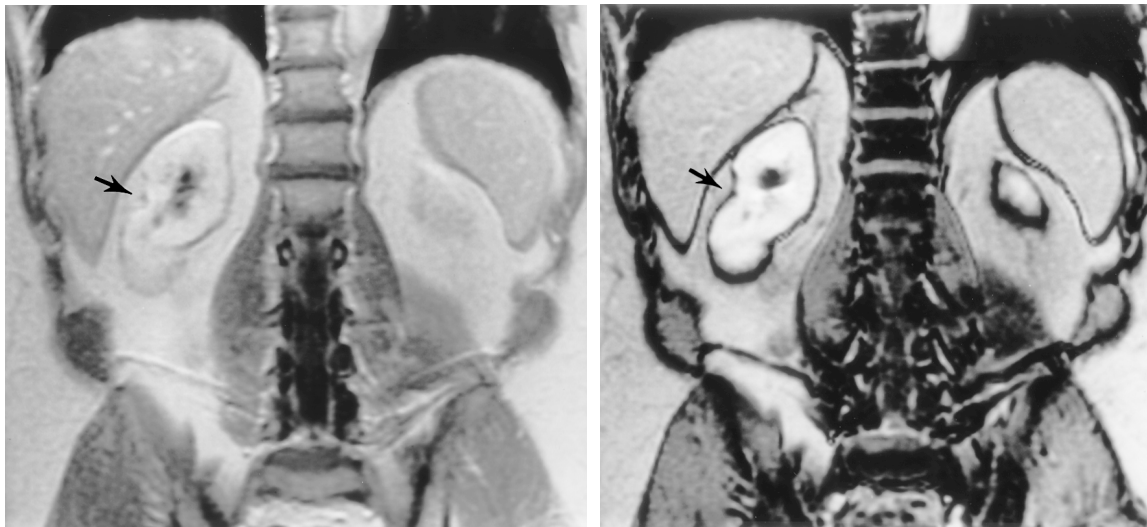
Chemical shift artifact can also be reduced by minimizing the signal contribution from lipids with the use of fat-suppression techniques such as spectral saturation.

Phase Cancellation.—The effects of chemical shift are most prominent in images obtained with gradient-echo pulse sequences, such as FMPSPGR. Because gradient-echo sequences are faster than spin-echo sequences, they can be used for dynamic imaging and applications that require breath-holding techniques. These imaging strategies have contributed to the rise in popularity of gradient-echo imaging of the body.

Traditional spin-echo imaging uses a 180° refocusing radio-frequency pulse applied at the center of the TE (1/2 TE). This pulse redirects the fat and water proton precessions or spins back into phase with respect to one other by the actual readout or TE (13). In contrast, gradient-echo sequences do not employ a 180° radio-frequency pulse to refocus the image signal. The lack of a 180° refocusing radio-frequency pulse in gradient-echo sequences results in the cycling of fat and water proton signals in and out of phase with respect to each other over time (5,14). Unlike repetition time, the TE (ie, the time the echo is sampled) plays a significant role in determining the relative degree of phase

differences between fat and water protons (ie, degree of chemical shift) occurring in the image and the amount of signal decay that occurs over time (5,9,14). At 1.5 T, fat and water signals precess in phase approximately every 4.4 msec; at 1.0 T, every 7.0 msec; and at 0.5 T, every 13.2 msec (5). At in-phase TE selections (eg, TE of 4.2 msec on a 1.5-T MR imager), the signal contributions of lipid and water protons are additive in their contributions to the resultant image. During other TEs, they become progressively more out of phase, with the peak occurring at the intermediate times of about 2.1 msec and 6.3 msec on a 1.5-T MR imager. In terms of image signal, a time component called T2* also comes into play as the TE lengthens. T2* is the amount of dephasing that arises from magnetic field inhomogeneities and causes the signal to decay over time (5). Use of longer TEs will result in less signal contributing to the image than if shorter TEs were used.

If the echo is sampled at a time (TE) when the fat and water signals are out of phase (Fig 9), only the difference in fat and water proton signals within the voxel contributes to the resultant image. If considerable fat signal is present, the tissue will manifest diminished signal intensity. This mixing of lipid and water signals within the voxel accounts for the improved visualization of visceral margins seen in out-of-phase gradient-echo images (Fig 10).



a. **b.**
Figure 9. In-phase FMPSPGR image (90/4.2, 90°) of a 57-year-old man with focal scarring of his right kidney more accurately demonstrates enhancement (a), compared with the out-of-phase FMPSPGR image (90/2.2, 90°) (b), which better delineates the renal contours. The out-of-phase gradient-echo image better delineates the focal scar in the middle of the right kidney (arrow).

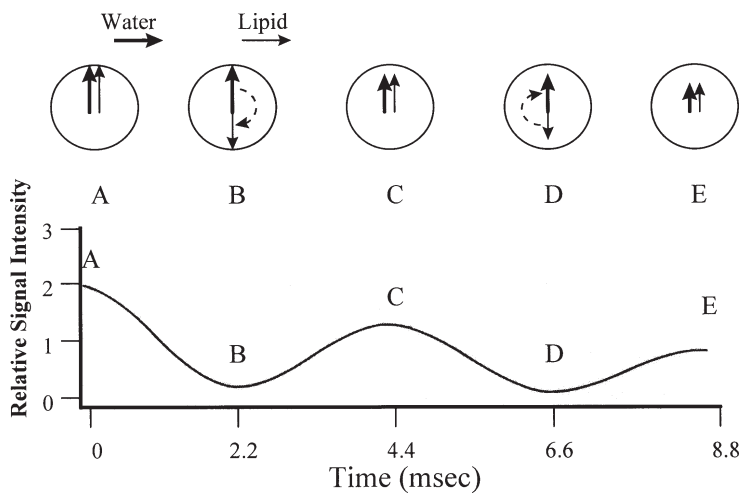


Figure 10. Schematic shows lipid and water protons precessing in and out of phase with respect to each other over time at 1.5 T. When lipid and water are in phase with each other, the net signal is additive, as shown at time points A, C, and E. Out-of-phase lipid and water signals nearly cancel each other out, as shown by the drop in the sine curve at time points B and D. The sine wave depicts the signal intensity within a voxel over time as the water and lipid protons oscillate between in phase and out of phase after the radio-frequency excitation pulse is delivered. The curve also drops in overall signal intensity due to T2* decay. (Modified and reprinted, with permission, from reference 5.)

Misexcitation.—Most of the structures of the human body have complex and irregular shapes. Smith et al (12) explored the effect of shape on chemical shift artifact. Using a coronal, oil-water interface, they were able to acquire oblique axial sections through the lipid slab in specific angles. They determined that chemical shift artifact was still apparent on oblique images with an angulation range of -20° to $+45^{\circ}$ from the lipid-water interface (12). This effect is postulated to occur because of chemical shift misregistration, as described earlier, and because of misexcitation occurring along the slice-selection direction. Misexcitation is the chemical shift that occurs during the slice selection of the pulse sequence. Misexcitation occurs because a frequency excitation pulse is applied while the slice-selection encoding gradient is being applied. The lipid region is chemically shifted along the slice-selection direction, which causes misexcitation of the lipid components and eventually results as a chemical shift artifact similar to misregistration (Fig 11) (5,12,15).

■ CLINICAL USE OF CHEMICAL SHIFT EFFECT

● Tissue Characterization

Neurologic Imaging.—In the head, fatty substances are mainly found in the orbits, bone marrow, and subcutaneous tissues of the skull. Lipid-containing intracranial masses, although rare, can be well demonstrated as hyperintense lesions on T1-weighted MR images (16,17). However, a number of other substances (including methemoglobin, protein, calcifications, and melanin) can also appear hyperintense on T1-weighted images (18–20). The coexistence of a chemical shift banding artifact around a high-signal-intensity focus on a T1-weighted image can help confirm the presence of lipid within the lesion. Because of the sharp lipid-cerebrospinal fluid or lipid-brain interface, chemical shift artifact can be noted in most intracranial lipomas (Fig 12) (10).

Teratomas and dermoids are other lipid-containing lesions that can occur inside the calvaria (21,22). Teratomas contain varying amounts of tissues from more than a single germ layer,

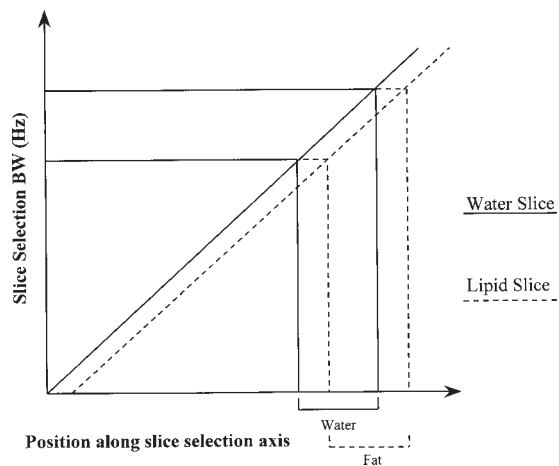


Figure 11. Schematic illustrates chemical shift misexcitation. During the slice-selection radio-frequency excitation pulse, protons are subjected to a range of frequencies or bandwidths (BW). The chemical shift between lipid and water actually shifts the lipid protons along the slice-selection axis. The lipid protons are excited in a position that is shifted slightly lower along the slice-selection axis than the water protons in the section, which causes a misexcitation to occur in the slice-selection direction. (Modified and reprinted, with permission, from reference 5.)

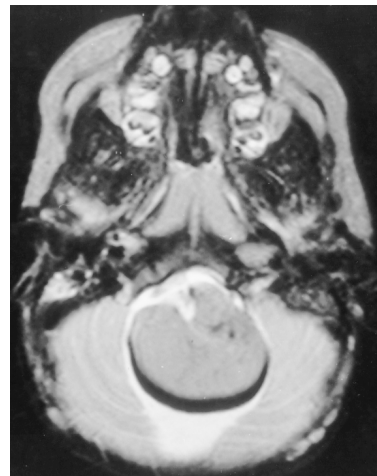
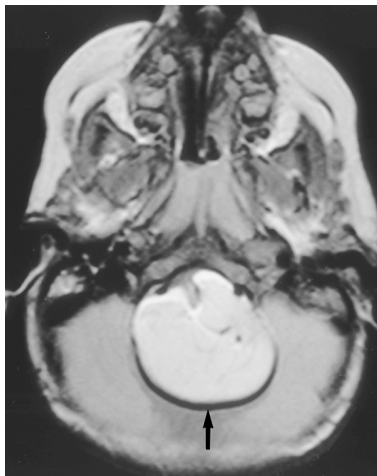
usually in a heterogeneous multiloculated mass that corresponds to the heterogeneous signal intensity depicted on MR images (21). Dermoids can show lipid material floating on top of the heavier water or proteinaceous material (21).

Body Imaging.—In gradient-echo MR imaging of the body, the selection of TE can be used to manipulate the relative contributions of fat and water signals for diagnostic purposes. For example, images obtained with out-of-phase TE will demonstrate visible or measurable decreases in signal intensity in tissues with considerable lipid, compared with the signal intensity on equivalent in-phase images. This use of “out-of-phase” gradient-echo sequences has become a popular technique for aiding in the diagnosis of both fatty infiltration and focal fat within the liver (23–27). A visible decrease in signal intensity will be apparent on out-of-phase gradient-echo images of these benign conditions (Fig 13). Because MR imaging can demonstrate signal intensity changes (due to fatty infiltration) quantitatively even at levels as low as 10% (28),



Figure 12. (a) Computed tomographic (CT) scan of a 1-year-old boy with a left external ear deformity shows an intracranial lipoma as a hypodense region (*). (b) Sagittal T1-weighted image (617/20) displays the fatty nature of the intracranial lipoma (*L*) as a homogeneously high-signal-intensity structure within the brain. (c) Axial proton-density-weighted image (3,500/20) obtained with inferior-to-superior frequency encoding shows a small amount of chemical shift artifact (arrow) occurring between the lipoma and the cerebrospinal fluid in the foramen magnum. (d) T2-weighted image (3,500/100) obtained with inferior-to-superior frequency encoding shows a much larger chemical shift artifact.

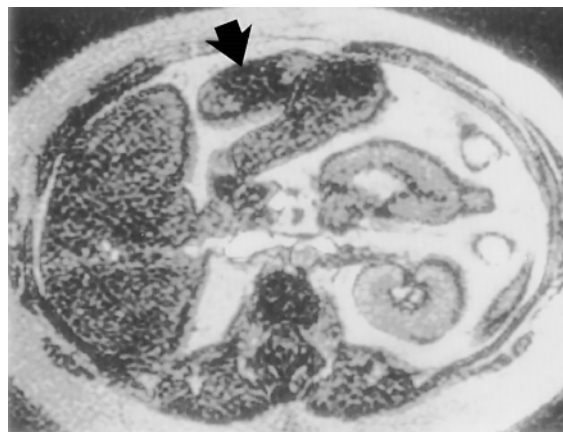
a.



b.

c.

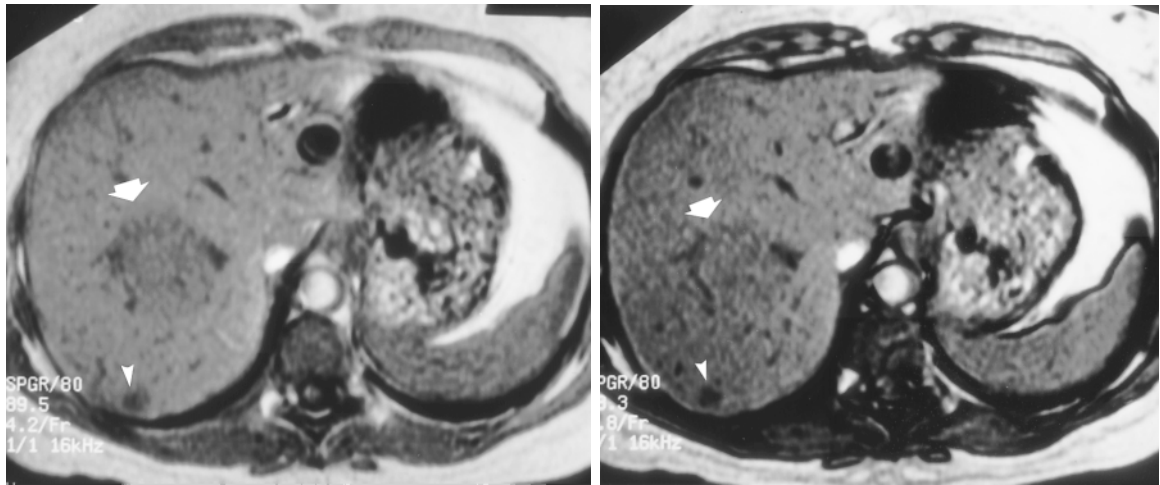
d.



a.

b.

Figure 13. (a) Axial T1-weighted image (400/10) of a 48-year-old woman, in whom CT had revealed a focal hypodense mass in the left lateral hepatic lobe, shows the lesion as a homogeneous, mildly high-signal-intensity area (arrow) without mass effect, findings suggestive of focal fat. The axial in-phase gradient-echo image (not shown) also depicted the lesion as hyperintense compared with the rest of the liver. (b) Axial out-of-phase FMPSPGR image (34/2.3, 90°) helps confirm that the mass is focal fat by demonstrating the same area as being very dark (arrow). Because of destructive interaction between fat and water signals on out-of-phase images, fatty lesions appear as a signal void.



a.

b.

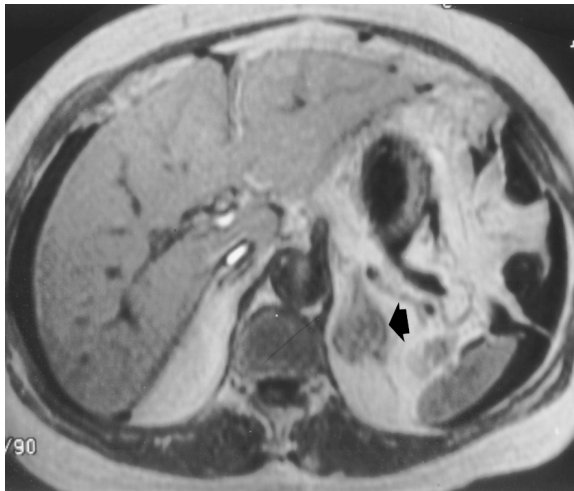
Figure 14. (a) Axial in-phase FMPSPGR T1-weighted, dynamic gadolinium-enhanced image (89.5/4.2, 80°) of a 46-year-old woman with diffuse fatty liver and focal nodular hyperplasia shows an enhancing mass, the focal nodular hyperplasia (arrow), in the right lobe of the liver (the mass was suspected from appearances on previous T1- and T2-weighted images). (b) Corresponding out-of-phase FMPSPGR image (78.3/2.3, 80°) poorly illustrates the mass (arrow). Because of suppression of the signal within surrounding fatty liver, the enhancing mass was less apparent on the out-of-phase image (b) than on the in-phase image (a). A small second lesion, a hemangioma (arrowhead), is incidentally noted just posterior to the focal nodular hyperplasia.

the selection of TE for dynamic imaging is important. An inappropriate TE selection may occasionally result in benign fatty infiltration of the liver and focal fat being mistaken for a malignancy or may mask the identity of the lesion (Fig 14) (24-27).

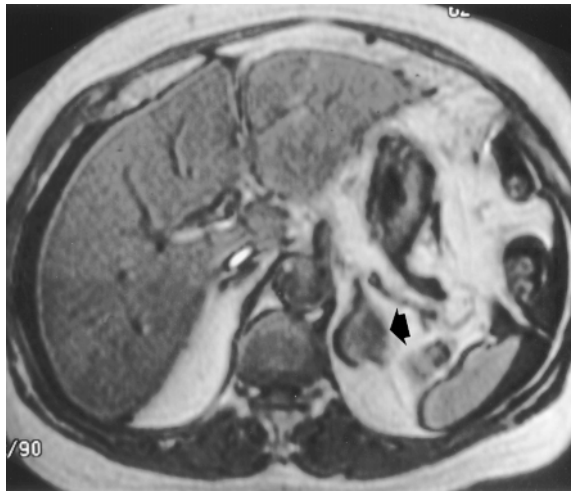
Chemical shift MR imaging has become a popular technique for diagnosing adrenal adenomas (29-42). Benign adrenal adenomas, which typically are composed of approximately 16% lipid based on in vitro studies (38), can demonstrate measurable differences in signal intensity when their appearance on in-phase gradient-echo images is compared with that on the out-of-phase counterparts (Fig 15). A decrease in signal intensity of greater than 20% within an adrenal mass on out-of-phase images helps confirm the diagnosis of an adrenal adenoma (40,42). Adrenal metastases (Fig 16), on the other hand, typically do not contain any significant lipid elements and

will not demonstrate an appreciable change in signal intensity with in-phase and out-of-phase chemical shift imaging (32,33,37,42). Some researchers have reported that chemical shift MR imaging is even more reliable than the measurement of Hounsfield units on nonenhanced CT scans for the confirmation of an adrenal adenoma (39). However, radiologists should be cautious about their conclusions in cases of subtle, heterogeneous signal changes and carefully inspect the mass for internal signal changes. In a recent report by Shifrin et al (43), a benign adrenal adenoma demonstrated apparent positive lipid signal changes on chemical shift images but also some heterogeneous signal changes due to a small focus of metastatic adenocarcinoma.

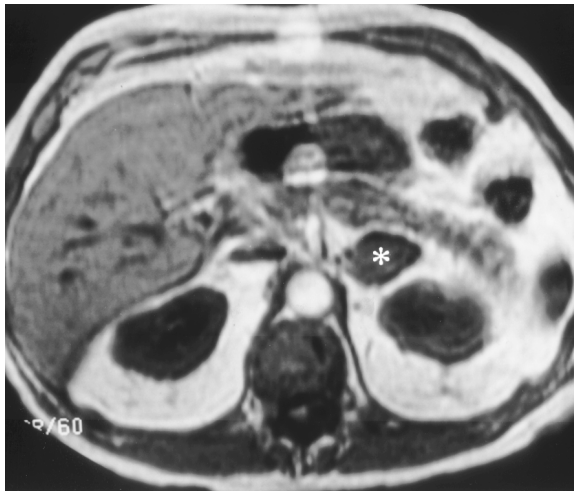
The speed of gradient-echo imaging has allowed for dynamic body MR imaging. Gradient-echo sequences that can be acquired during a brief breath hold provide the temporal resolution needed to evaluate tissue enhancement following administration of a contrast agent (Fig 17) (13,28). In an effort to decrease the



15a.



15b.

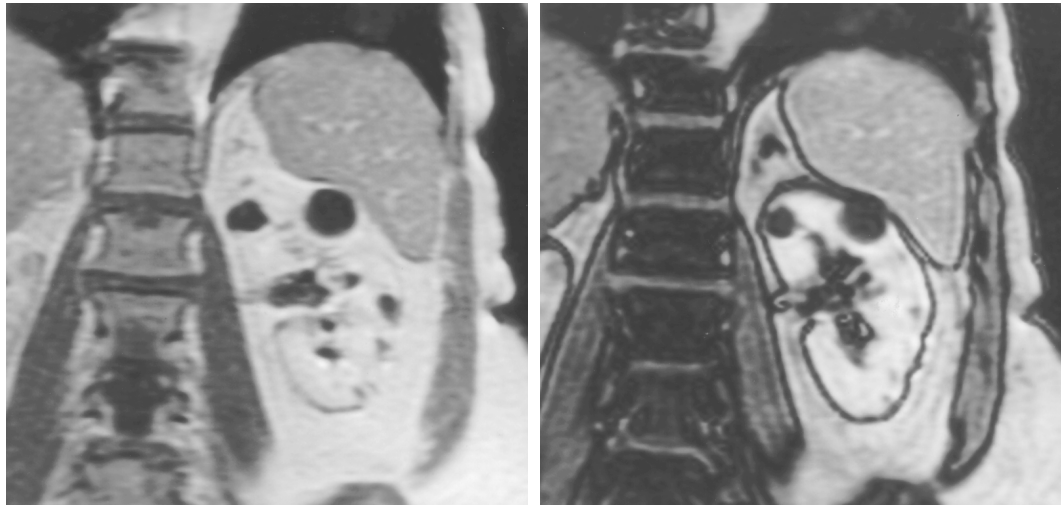


16a.



16b.

Figures 15, 16. (15) Axial in-phase FMPSPGR (89/4.2, 90°) (a) and out-of-phase FMPSPGR (89/3.1, 90°) (b) images of a 62-year-old woman show a 3-cm left adrenal mass, which had lower signal intensity (arrow) with the out-of-phase pulse sequence. Region-of-interest measurements of the mass were performed for both images. A substantial difference in mean signal intensity was measured between the images (in phase = 115, out of phase = 66; 42% decrease in signal intensity), which helped confirm the presence of fat within the lesion and the diagnosis of benign adrenal adenoma. (16) Axial in-phase FMPSPGR (74/4.2, 60°) (a) and out-of-phase (74/2.3, 60°) (b) images of a 76-year-old man with metastatic non-small cell and squamous cell carcinoma of the lung demonstrate a left adrenal mass (*). No differences in signal are seen on the two images. Metastases generally do not contain fat and do not exhibit the signal loss caused by chemical shift effects.



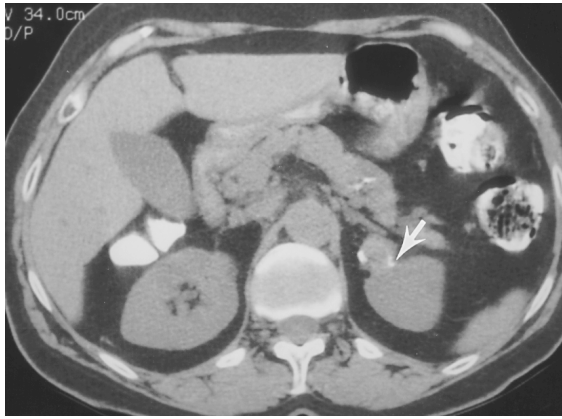
a. **b.**
Figure 17. (a) Coronal in-phase FMPSPGR image (57/4.2, 80°) of a 70-year-old woman obtained after intravenous administration of a gadolinium-chelate contrast agent reveals several nonenhancing simple renal cysts in the left kidney. (b) Coronal out-of-phase image (57.4/2.4, 80°) better delineates the renal margins and relative locations of the cysts.



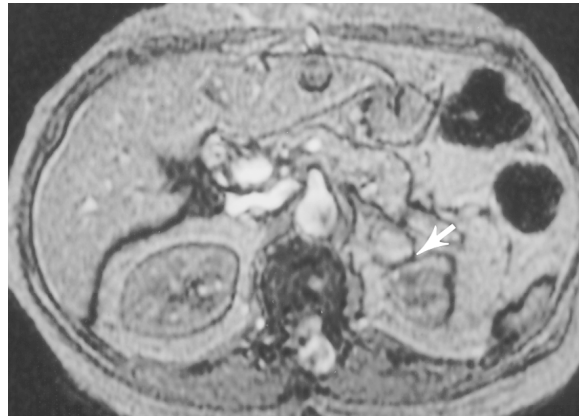
a. **b.**
Figure 18. (a) Coronal gadolinium-enhanced in-phase FMPSPGR image (90/4.2, 90°) of a 44-year-old woman demonstrates an enhancing renal mass (arrow). (Previous CT scan revealed a 2-cm complex low-attenuation lesion in the inferior pole of the left kidney that was not consistent with a simple renal cyst.) (b) Coronal out-of-phase image (90/2.3, 90°) obtained less than 30 seconds after a reveals a dramatic reduction in the signal intensity of the mass, despite the gadolinium enhancement.

time needed for the breath hold, gradient-echo sequences are commonly performed with the shortest possible TE, which frequently is an out-of-phase TE (4,41,44). Use of only out-of-

phase images, however, may mask lesions in the liver (Fig 14). Mitchell et al (44) recently described a similar phenomenon in the kidney. They reported paradoxical suppression of signal intensity in angiomyolipomas (Fig 18) on out-of-phase gradient-echo images obtained after administration of a gadolinium-based con-



19a.



19b.



20.

Figures 19, 20. (19a) Axial CT scan of a 69-year-old woman shows a mass in the left adrenal gland that appears to invade the left kidney (arrow). (19b) On an out-of-phase FMPSGR image (90/6.3, 90°), a black boundary surrounding the adrenal gland and the kidney can be seen. On a subsequent follow-up MR image (not shown), the left adrenal mass had decreased in size, a finding consistent with an adrenal hemorrhage. (20) Sagittal out-of-phase FMPSGR image (50/6, 90°) of a 57-year-old man with known colon cancer shows a mass (*m*) invading through the Gerota fascia and into the anterior aspect of the lower pole of the right kidney (arrow), as evidenced by the interruption of the dark cortical line that demarcates the renal margin. The mass has also invaded the liver, as shown by the absence of the dark line that should be seen along the inferior margin of the liver.

trast agent. For these reasons, one should be judicious in the selection of the TE for dynamic contrast material-enhanced imaging, especially if an assessment of signal intensity is desired. A good example that illustrates the importance of using an in-phase TE to evaluate contrast media enhancement patterns is the case in Figure 14, in which the patient had both focal nodular hyperplasia and diffuse fatty infiltration of the liver. The mass of focal nodular hyperplasia was much more conspicuous on the in-phase images than on the out-of-phase images, possibly because of the signal suppression in adjacent enhancing fatty liver. Because out-of-phase images can be used to confirm contrast material enhancement within lipomatous tumors such as angiomyolipomas (Fig 18), they should be included, albeit at the end of the dynamic imaging examination.

The out-of-phase images also can be very helpful because they afford improved anatomic delineation of peripheral lesions that border on lipid-water interfaces (Fig 17).

● Visceral Delineation

Chemical shift can be used as a tool for delineating structures that are surrounded by fat. Out-of-phase images can aid in the demarcation of the renal contour (Fig 9), the margin of the adrenal glands (Fig 19), and the liver edge (Fig 20). Gradient-echo images that use out-of-phase chemical shift demonstrate dark lines around organs embedded in fat. These dark lines are created by the phase cancellation of the fat and water signals that exist within the voxels of the lipid-water interface. The width of the dark lines can be accentuated by increasing the field of view.

Use of a narrower bandwidth will also increase the chemical shift banding seen on the images (2,5). However, narrowing the bandwidth may increase the TE of the sequence or limit the number of sections that can be acquired.

■ CONCLUSIONS

Chemical shift principle can be applied to help characterize and delineate tissues in the head and body. The acquisition of both in- and out-of-phase images, requiring only 1-2 minutes of imaging time, can be added to almost any MR imaging protocol. The information from these quick sequences can often aid in the diagnosis, either by delineating visceral contours or by demonstrating the presence of lipid elements. This quick imaging technique is a valuable adjunct to a radiologist's bag of tricks.

■ REFERENCES

1. Rholl KS, Lee JKT, Heiken JP, Ling D, Glazer HS. Primary bladder carcinoma: evaluation with MR imaging. *Radiology* 1987; 163:117-121.
2. Simon JH, Foster TH, Ketonen L, et al. Reduced-bandwidth MR imaging of the head at 1.5 T. *Radiology* 1989; 172:771-775.
3. Herrick RC, Hayman LA, Taber KH, Diaz-Marchan PJ, Kuo MD. Artifacts and pitfalls in MR imaging of the orbit: a clinical review. *RadioGraphics* 1997; 17:707-724.
4. Rofsky NM, Weinreb JC, Ambrosino MM, Safir J, Krinsky G. Comparison between in-phase and opposed-phase T1-weighted breath-hold FLASH sequences for hepatic imaging. *J Comput Assist Tomogr* 1996; 20:230-235.
5. Szumowski J, Simon JH. Proton chemical shift imaging. In: Stark D, Bradley W, eds. *Magnetic resonance imaging*. St Louis, Mo: Mosby-Year Book, 1994; 479-521.
6. Babcock EE, Brateman L, Weinreb JC, Horner SD, Nunnally RL. Edge artifacts in MR images: chemical shift effect. *J Comput Assist Tomogr* 1985; 9:252-257.
7. Brateman L. Chemical shift imaging: a review. *AJR* 1986; 146:971-980.
8. Simon JH, Szumowski J. Proton (fat/water) chemical shift imaging in magnetic resonance imaging. *Invest Radiol* 1992; 27:865-874.
9. Parizel PM, van Hasselt BAAM, van den Hauwe L, Van Goethem JWM, De Schepper AMA. Understanding chemical shift induced boundary artefacts as a function of field strength: influence of imaging parameters (bandwidth, field-of-view, and matrix size). *Eur J Radiol* 1994; 18:158-164.
10. Smith AS, Weinstein MA, Hurst GC, DeRemer DR, Cole RA, Duchesneau PM. Intracranial chemical-shift artifacts on MR images of the brain: observations and relation to sampling bandwidth. *AJR* 1990; 154:1275-1283.
11. Edelman RR, Hesselink JR, Zlatkin MB. *Clinical magnetic resonance imaging*. Philadelphia, Pa: Saunders, 1996.
12. Smith RC, Lange RC, McCarthy SM. Chemical shift artifact: dependence on shape and orientation of the lipid-water interface. *Radiology* 1991; 181:225-229.
13. Mitchell DG. Chemical shift magnetic resonance imaging: applications in the abdomen and pelvis. *Top Magn Reson Imaging* 1992; 4:46-63.
14. Wehrli FW, Perkins TG, Shimakawa A, Roberts F. Chemical shift-induced amplitude modulations in images obtained with gradient refocusing. *Magn Reson Imaging* 1987; 5:157-158.
15. Lee HK, Nalcioglu O, Buxton RB. Correction for chemical-shift artifacts in 19F imaging of PFOB: simultaneous multislice imaging. *Magn Reson Med* 1991; 21:21-29.
16. Dooks GC, Hricak H, Sollitto RA, Higgins CB. Lipomatous tumors and tumors with fatty component: MR imaging potential and comparison of MR and CT results. *Radiology* 1985; 157:479-483.
17. Truwit CL, Barkovich AJ. Pathogenesis of intracranial lipoma: an MR study in 42 patients. *AJR* 1990; 155:855-864.
18. Eghwudjakpor PO, Kurisaka M, Fukuoka M, Mori K. Intracranial lipomas: current perspectives in their diagnosis and treatment. *Br J Neurosurg* 1992; 6:139-144.
19. Henkelman RM, Watts JF, Kucharczyk W. High signal intensity in MR images of calcified brain tissue. *Radiology* 1991; 179:199-206.

20. Bradley WG. MR appearance of hemorrhage in the brain. *Radiology* 1993; 189:15-26.
21. Smirniotopoulos JG, Chiechi MV. Teratomas, dermoids, and epidermoids of the head and neck. *RadioGraphics* 1995; 15:1437-1455.
22. Zee C, Segall H, Apuzzo M, et al. MR imaging of pineal region neoplasms. *J Comput Assist Tomogr* 1991; 15:56-63.
23. Martin J, Sentis M, Zidan A, Donosol L, Puig J, Falco J, Bela R. Fatty metamorphosis of hepatocellular carcinoma: detection with chemical shift gradient-echo MR imaging. *Radiology* 1995; 195:125-130.
24. Mitchell DG. Focal manifestations of diffuse liver disease at MR imaging. *Radiology* 1992; 185:1-11.
25. Mitchell DG, Palazzo J, Hann HYL, Rifkin MD, Burk DL, Rubin R. Hepatocellular tumors with high signal on T1-weighted MR images: chemical shift MR imaging and histologic correlation. *J Comput Assist Tomogr* 1991; 15:762-769.
26. Hoyumpa AM, Greene HL, Dunn GD, Schenker S. Fatty liver: biochemical and clinical considerations. *Am J Dig Dis* 1975; 20:1142-1170.
27. Lewis E, Bernardino ME, Barnes PA, Parvey HR, Soo CS, Chuang VP. The fatty liver: pitfalls in the CT and angiographic evaluation of metastatic disease. *J Comput Assist Tomogr* 1983; 7:235-241.
28. Mitchell DG, Kim I, Chang TS, et al. Chemical shift phase-difference and suppression magnetic resonance imaging techniques in animals, phantoms, and humans. *Invest Radiol* 1991; 26:1041-1052.
29. Mitchell DG, Crovello M, Matteucci T, Petersen RO, Miettinen MM. Benign adrenocortical masses: diagnosis with chemical shift MR imaging. *Radiology* 1992; 185:345-351.
30. Krestin GP. Magnetic resonance imaging of the kidneys: current status. *Magn Reson Q* 1994; 10:2-21.
31. Tsushima Y, Ishizaka H, Matsumoto M. Adrenal masses: differentiation with chemical shift, fast low-angle shot MR imaging. *Radiology* 1993; 186:705-709.
32. Bilbey JH, McLoughlin RF, Kurkjian PS, et al. MR imaging of adrenal masses: value of chemical-shift imaging for distinguishing adenomas from other tumors. *AJR* 1995; 164:637-642.
33. Outwater EK, Siegelman ES, Radecki PD, Piccoli CW, Mitchell DG. Distinction between benign and malignant adrenal masses: value of T1-weighted chemical-shift MR imaging. *AJR* 1995; 165:579-583.
34. Korobkin M, Lombardi TJ, Aisen AM, et al. Characterization of adrenal masses with chemical shift and gadolinium-enhanced MR imaging. *Radiology* 1995; 197:411-418.
35. Outwater EK, Siegelman ES, Huang AB, Birnbaum BA. Adrenal masses: correlation between CT attenuated value and chemical shift ratio at MR imaging with in-phase and opposed-phase sequences. *Radiology* 1996; 200:749-752.
36. Schwartz LH, Panicek DM, Koutcher JA, et al. Adrenal masses in patients with malignancy: prospective comparison of echo-planar, fast spin-echo, and chemical shift MR imaging. *Radiology* 1995; 197:421-425.
37. Krestin GP, Steinbrich W, Friedmann G. Adrenal masses: evaluation with fast gradient-echo MR imaging and Gd-DTPA-enhanced dynamic studies. *Radiology* 1989; 171:675-680.
38. Leroy-Willig A, Bittoun J, Luton JP, et al. In vivo MR spectroscopic imaging of the adrenal glands: distinction between adenomas and carcinomas larger than 15 mm based on lipid content. *AJR* 1989; 153:771-773.
39. McNichols MMJ, Lee MJ, Mayo-Smith WW, Hahn PF, Boland GW, Mueller PR. An imaging algorithm for the differential diagnosis of adrenal adenomas and metastases. *AJR* 1995; 165:1453-1459.
40. Mayo-Smith WW, Lee MJ, McNichols MMJ, Hahn PF, Boland GW, Saini S. Characterization of adrenal masses (<5 cm) by use of chemical shift MR imaging: observer performance versus quantitative measures. *AJR* 1995; 165:91-95.
41. Korobkin M, Giordano TJ, Brodeur FJ, et al. Adrenal adenomas: relationship between histologic lipid and CT and MR findings. *Radiology* 1996; 200:743-747.
42. Reinig JW, Stutley JE, Leonhardt CM, Spicer KM, Margolis M, Caldwell CB. Differentiation of adrenal masses with MR imaging: comparison of techniques. *Radiology* 1994; 192:41-46.
43. Shifrin RY, Bechtold RE, Scharling ES. Metastatic adenocarcinoma within an adrenal adenoma: detection with chemical shift imaging. *AJR* 1996; 167:891-892.
44. Mitchell DG, Stolpen AH, Siegelman ES, Bolinger L, Outwater EK. Fatty tissue on opposed-phase MR images: paradoxical suppression of signal intensity by paramagnetic contrast agents. *Radiology* 1996; 198:351-357.